

## PREDICTIONS OF FRACTURE RESISTANCE OF SPRUCE WOOD UNDER MIXED-MODE LOADING USING NON-LOCAL FRACTURE THEORY AND NUMERICAL MODELLING

MAREK ROMANOWICZ

*Bialystok University of Technology, Department of Mechanical Engineering, Bialystok, Poland  
e-mail: m.romanowicz@pb.edu.pl*

A novel analytical model to predict fracture resistance of a quasi-brittle material, like wood, is presented. The model is based on a scaling parameter introduced into the non-local fracture theory to take into account the specimen size effect on the development of the damage zone. An expression for length of the critical process zone, which can be used in damage tolerant design of wooden structures is derived from this theory. The model is validated with mixed-mode bending tests. A numerical analysis using cohesive elements is performed to understand the role of specimen size in the development of the damage zone. The analytical predictions of the fracture resistance and the critical process zone length for wood are compared with numerical results and experimental data available in the literature.

*Keywords:* mixed-mode bending test, process zone length, resistance curve, fracture criteria, cohesive zone model

### 1. Introduction

Two approaches have been reported in the literature to consider damage processes occurring ahead of the crack tip in quasi-brittle materials: the concept of cohesive fracture models originated by Barenblatt (1962) and Dugdale (1960) and the concept of non-local fracture models introduced by Novozhilov (1969). The first approach is through decohesion of the upper and lower surfaces of the process zone ahead of the crack tip. The second approach involves averaging of the stresses over this zone. It can be seen in Fig. 1 that the averaged stress over the length  $L_{cz}$  cannot exceed the strength of the material in the non-local model, whereas the cohesive model assumes a gradual loss of stiffness over the length  $L_{cz}$ .

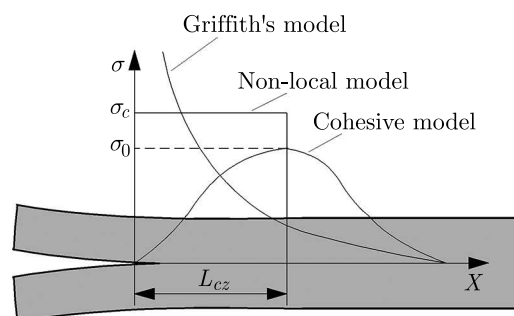


Fig. 1. Stress distribution ahead of the crack tip

Development of the fracture process zone (FPZ) in a quasi-brittle material like wood leads to a stable crack growth before the complete fracture (Morel *et al.*, 2005). The ability to predict the stable growth of a pre-existing crack under a mixed-mode loading is a key requirement in damage tolerant design of wooden structures. In recent studies (de Moura *et al.*, 2010; Phan *et*

*al.*, 2016), the initiation and propagation fracture toughnesses of wood under the mixed-mode loading have been typically described by an empirical power law combining energy release rates in mode I and II with their critical values, i.e.  $(G_I/G_{Ic})^m + (G_{II}/G_{IIc})^n = 1$ , where  $m$ ,  $n$  are constants.

Originally developed by Reeder and Crews (1990) to study the mixed-mode interlaminar fracture toughness of composite laminates, the mixed-mode bending test (MMB) was also used to investigate the resistance to crack growth in wood (de Moura *et al.*, 2010; Phan *et al.*, 2016). The use of this test is justified by the fact that it is capable of keeping a constant mixed-mode ratio during crack growth. In the framework of equivalent linear elastic fracture mechanics (LEFM) proposed by Bazant and Kazemi (1990), the secant compliance estimated from any point of the load-displacement curve corresponds to the initial elastic compliance of the cracked specimen, in which the crack length is given by the actual one plus a correction due to the FPZ development, i.e.  $a_{eq} = a_0 + \Delta a$ . Using this approach, it has been found that variations of mode I and mode II energy release rates with crack length ( $R$ -curves) for wood follow an initially increasing trend before reaching a plateau, which indicates the appearance of self-similar propagation of the main crack with its critical FPZ.

Numerous analytical and numerical models have been proposed to calculate the variation of the energy release rate directly from the MMB test data. Within the framework of simple beam theory, the cracked specimen is considered as an assemblage of three rigidly connected sublaminates (Reeder and Crews, 1990). In order to take into account the effects of deflections and rotations at the crack tip, crack length corrections are introduced into the simple beam theory (Williams, 1989; Wang and Williams, 1992). According to enhanced beam theory, the two sublaminates are partially connected by a deformable interface to take into account the crack propagation. Splitting of the two sublaminates is modeled by applying elastic brittle (Bennati *et al.*, 2013a,b) or elastic damaging constitutive laws (Xie *et al.*, 2016a,b). Compared to the simple beam theory, the enhanced beam theory is capable of capturing the pre-peak nonlinearity of load-displacement response. However, due to the assumptions of the beam theory, it over-predicts the pre-peak stiffness and process zone length. Numerical simulations of the MMB test are typically performed in the framework of the finite element method by using the virtual crack closure technique (Xie and Biggers, 2006; Oliveira *et al.*, 2007) or the cohesive zone model (Alfano and Crisfield, 2001; Camanho and Dávila, 2002). The main difference between them is that the latter has the capability to model damage mechanisms, whereas the former does not. However, since numerical predictions are mesh-dependent, care must be taken to ensure that element sizes are capable of capturing strain and stress gradients near the crack tip.

The objective of this paper is to show that the non-local fracture theory proposed by Seweryn and Mróz (1998) is capable of predicting the propagation fracture toughness of wood under mixed-mode loading conditions. To date, only the initiation fracture toughness of wood has been analyzed by using this fracture theory (e.g. Romanowicz, 2019). In previous papers, it has been assumed that the compliance within the damage zone and the process zone length are material properties. Extension of the non-local fracture theory to the study of the crack propagation resistance requires redefining these concepts. In this paper, the quasi-brittle fracture characteristics predicted from the extended non-local theory are verified against MMB test data available in the literature and numerical simulations accounting for cohesive properties of wood.

## 2. Non-local theory of quasi-brittle fracture

In this Section, a novel analytical approach for estimating the critical process zone length  $L_{cz}$  based on the non-local fracture theory is presented. According to the non-local fracture theory

proposed by Seweryn and Mróz (1998), a crack starts to grow when a stress function  $R(\sigma_\theta, \tau_{r\theta})$  averaged over the process zone length  $l_{cz}$  reaches the maximum value

$$\max \left( \frac{1}{l} \int_0^{l_{cz}} R(\sigma_\theta, \tau_{r\theta}) dr \right) = 1 \quad (2.1)$$

where  $\sigma_\theta, \tau_{r\theta}$  are the stress components in a polar coordinate system  $(r, \theta)$  originated at the crack tip. This fracture theory is motivated by the fact that the stress distribution within the process zone is difficult to estimate precisely. For this reason, it is convenient to use the average value of stress. For a damage zone weakened by microcracks, Seweryn and Mróz (1998) proposed the following elliptic function for calculating the fracture toughness

$$R(\sigma_\theta, \tau_{r\theta}) = \sqrt{\left(\frac{\sigma_\theta}{\sigma_c}\right)^2 + \rho \left(\frac{\tau_{r\theta}}{\sigma_c}\right)^2} \quad (2.2)$$

where  $\sigma_c$  is the tensile strength representing the ratio of the sliding and extensional compliance of the material within the damage zone. Maximizing the average value of  $R(\sigma_\theta, \tau_{r\theta})$  with respect to  $\theta$ , the location of the critical plane is determined. The non-local model of crack propagation is formulated by assuming that the process zone length is much less than the crack length. On this assumption, the stress distribution associated with damage mechanisms occurring ahead of the crack tip is dominated by a singular crack tip solution of the type  $r^{-0.5}$ . It was reported by Romanowicz (2019) that the stress function (2.2) has for orthotropic materials its maximum at  $\theta = 0^\circ$  if the reinforcement direction coincided with the crack axis. Thus, in the case of self-similar crack growth, stress function (2.2) can be expressed as

$$R(\sigma_\theta, \tau_{r\theta}) = \frac{1}{\sigma_c} \sqrt{\frac{K_I^2}{2\pi r} + \rho \frac{K_{II}^2}{2\pi r}} \quad (2.3)$$

where  $K_I, K_{II}$  are stress intensity factors for pure opening and pure sliding modes, respectively. Substituting (2.3) into (2.1) and integrating from  $r = 0$  to  $r = l_{cz}$  the non-local criterion of crack propagation is given in terms of stress intensity factors as

$$K_I^2 + \rho K_{II}^2 = \frac{l_{cz} \sigma_c^2 \pi}{2} \quad (2.4)$$

On the assumptions of LEFM, the stress intensity factors for orthotropic materials are related to strain energy release rates by the relationship proposed by Sih *et al.* (1965)

$$G = G_I + G_{II} = \frac{K_I^2}{E_I} + \frac{K_{II}^2}{E_{II}} \quad (2.5)$$

where:  $G, G_I, G_{II}$  are total, mode I and II energy release rates, respectively,  $E_I, E_{II}$  are generalized elastic moduli. The procedure for calculating  $E_I, E_{II}$  is provided in Appendix A. One potential limitation in application of Eq. (2.4) is that the compliance ratio is, in general, an unknown parameter. In order to overcome this limitation, the ratio can be calibrated by fitting theoretical predictions to experimental data. In this paper, the compliance ratio is thus defined as some multiple of the ratio between  $E_I$  and  $E_{II}$

$$\rho = \frac{E_I}{nE_{II}} \quad (2.6)$$

where  $n$  is an empirical parameter. In the previous papers on the initiation fracture toughness of wood (Romanowicz, 2019), the compliance ratio was assumed to be  $\rho = (K_{Ic}/K_{IIc})^2$ , where

$K_{Ic}$  and  $K_{IIc}$  are mode I and II critical stress intensity factors. By using Eqs. (2.5) and (2.6), the non-local criterion of crack propagation (2.4) can be now expressed in terms of mode I and II energy release rates as

$$nG_I + G_{II} = \frac{l_{cz}\sigma_c^2\pi n}{2E_I} \quad (2.7)$$

When the process zone is fully developed  $l_{cz} = L_{cz}$ , the fracture resistance can be estimated from the strain energy release rate as  $G = G_R$ . Formally, substituting  $l_{cz} = L_{cz}$  into (2.7) means that the non-local criterion predicts the moment of complete fracture. In this paper, the value of  $L_{cz}$  is chosen so as to make non-local criterion (2.7) equivalent to the semi-empirical mixed-mode propagation criterion proposed by Benzeggagh and Kenane (1996). According to this criterion, the total fracture resistance is a power function of the mixed-mode ratio  $G_{II}/G$

$$G_R = G_{IR} + (G_{IIR} - G_{IR})\left(\frac{G_{II}}{G}\right)^m \quad (2.8)$$

where:  $G_R$ ,  $G_{IR}$ ,  $G_{IIR}$  are total, mode I and II fracture resistances,  $m$  is an empirical parameter. Since the strength  $\sigma_c$  and modulus  $E_I$  are constants, it is reasonable to assume that the length  $L_{cz}$  occurring in non-local criterion (2.7) should follow the same trend as the fracture resistance  $G_R$  predicted by the Benzeggagh and Kenane criterion. It should be noted that it is possible to rewrite the Benzeggagh and Kenane criterion so that the left hand sides of Eqs. (2.7) and (2.8) are equal when  $l_{cz} = L_{cz}$

$$nG_{IR} + G_{IIR} = nG_{IR} + (G_{IIR} - G_{IR})\left(\frac{G_{II}}{G}\right)^m \quad (2.9)$$

Finally, by equating the right hand sides of Eqs. (2.7) and (2.9), the length of the fully developed process zone can be written as a power function of the mixed-mode ratio  $G_{II}/G$

$$L_{cz} = \frac{2E_I}{\sigma_c^2\pi n} \left[ nG_{IR} + (G_{IIR} - G_{IR})\left(\frac{G_{II}}{G}\right)^m \right] \quad (2.10)$$

Substituting (2.10) into (2.7), the non-local criterion takes the form of the Benzeggagh and Kenane criterion. Mode I and II process zone lengths are calculated by setting  $G_{II}/G = 0$  and  $G_{II}/G = 1$  in (2.10), as follows

$$L_{Icz} = \frac{2E_I G_{IR}}{\sigma_c^2\pi} \quad L_{IIcz} = \frac{2E_I}{\sigma_c^2\pi n} [G_{IIR} + (n-1)G_{IR}] \quad (2.11)$$

Figure 2 shows solutions of the dimensionless characteristic length  $L_{cz}$  for a fixed value of  $m$  and various values of  $n$ . It is interesting to note that the variation of process zone length with ratio  $G_{II}/G$  becomes smaller as  $n$  increases and for large values of  $n$ , a constant process zone length equal to  $L_{Icz}$  is observed. From Eqs. (2.11), mode I process zone length is not influenced by the parameter  $n$  and when  $n = 1$ , mode II process zone length can be written in terms of  $G_{IIR}$  only. Based on these findings, the parameter  $n$  controls the value of mode II process zone length and the steepness of the curve describing the relationship between the process zone length and the mixed-mode ratio. It can be interpreted as a scaling parameter for the ratio of the sliding and extensional compliance of the material within the damage zone.

### 3. Finite element simulations of quasi-brittle fracture

In this Section, the finite element implementation of a bilinear cohesive zone model proposed by Alfano and Crisfield (2001) and Camanho and Dávila (2002) is presented to predict damage

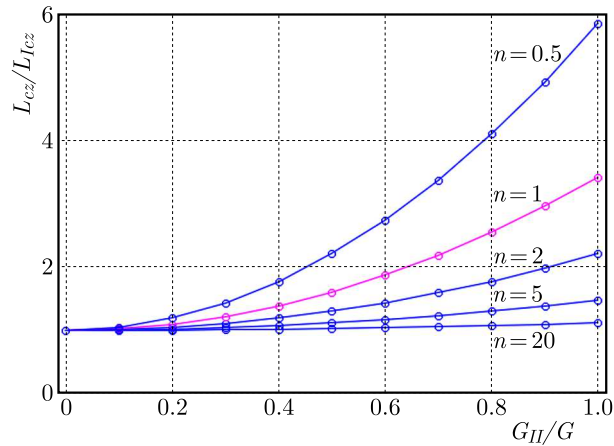


Fig. 2. Effect of the parameter  $n$  on the variation of dimensionless process zone length with the mixed-mode ratio

evolution in wood. Finite element analyses have been conducted under mode I, mode II and mixed-mode loading using the double cantilever beam (DCB), end notched flexure (ENF) and mixed-mode bending (MMB) specimens, respectively. The deformed finite element meshes and boundary conditions corresponding to these cases are shown in Fig. 3. The MMB test uses a lever to simultaneously apply the loads which are similar to those applied to the DCB and ENF tests. Mixed-mode ratios are controlled by the lever length  $c$ . Five different lever lengths  $c = 160, 200, 235, 335, 435$  mm are studied. The length  $2L$ , width  $B$  and thickness  $2h$  of the specimens are 750 mm, 30 mm and 30 mm, respectively. The length of the support span  $2l$  is fixed in all tests at 650 mm. The length of the pre-crack  $a_0$  measured from the beam support point is 227 mm. These specimens correspond to those used in experiments performed by Phan *et al.* (2016) on Norway spruce in the TL crack system. The specimen material is assumed to be linearly elastic and orthotropic (Table 1). The specimen geometry is meshed with two-dimensional plane strain 4 node elements in Ansys (PLANE182). The mesh is refined along a predefined crack path located at the midplane of the specimen. The elements ahead of the crack tip have the length 0.6 mm. Frictionless contact is assigned between the crack surfaces. The MMB test apparatus is modeled explicitly using beam elements (BEAM188) with material properties much stiffer than those of the specimen. In order to connect the rigid beam elements with the plane elements and to enforce the appropriate boundary conditions, multi-point constraints (MPC184) are used.

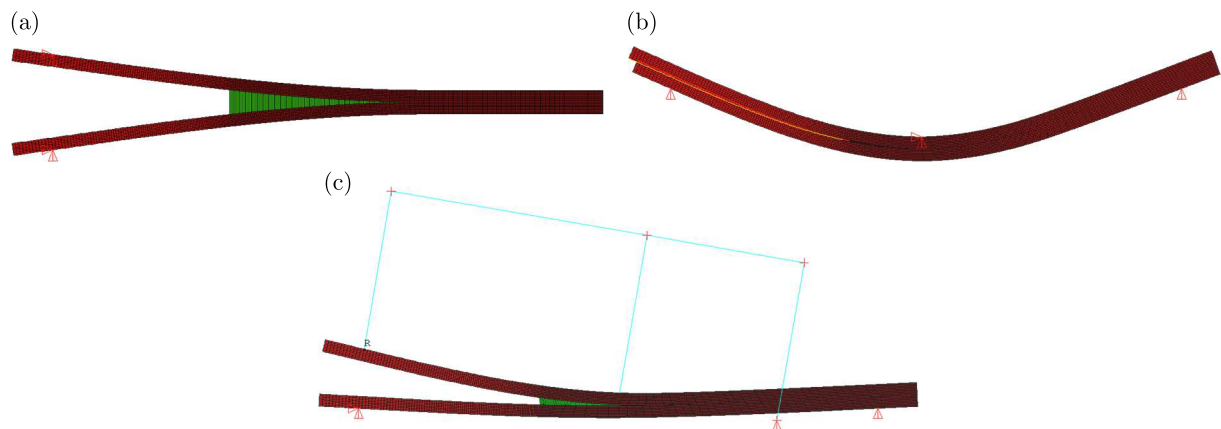


Fig. 3. Finite element meshes and boundary conditions used in the simulations: (a) DCB test, (b) ENF test, (c) MMB test

**Table 1.** Elastic properties of Norway spruce (Dourado *et al.*, 2008) and its tensile strength in the tangential direction (Pedersen *et al.*, 2003)

$E_L$ [MPa]	$E_R$ [MPa]	$E_T$ [MPa]	$\nu_{TL}$ [-]	$\nu_{RL}$ [-]	$\nu_{TR}$ [-]	$G_{TL}$ [MPa]	$G_{RT}$ [MPa]	$G_{RL}$ [MPa]	$\sigma_c^T$ [MPa]
9900	730	410	0.018	0.032	0.306	610	22	500	2.7

Crack propagation is modeled by using zero-thickness cohesive elements (INTER202) based on a bilinear traction-separation constitutive relationship,  $\sigma_i = \sigma_i(\delta_i)$ , with  $i = I, II$ . The response of cohesive elements is linear-elastic up to the onset of damage. After the damage onset, the interface elements start losing their stiffness linearly. When the stiffness of the cohesive elements reduces to zero, crack growth occurs. Mode I and mode II energy release rates are calculated in Ansys as

$$G_I = \int_0^{\delta_I} \sigma_I d\delta_I \quad G_{II} = \int_0^{\delta_{II}} \sigma_{II} d\delta_{II} \quad (3.1)$$

The mixed-mode cohesive zone model implemented here requires two cohesive strengths  $\sigma_I^0$  and  $\sigma_{II}^0$ , two separations at the onset of damage  $\delta_I^0$  and  $\delta_{II}^0$ , and two separations at the moment of fracture  $\delta_I^c$  and  $\delta_{II}^c$  to predict the evolution of damage. In order to ensure that both tractions vanish simultaneously at complete separation, the ratios  $\delta_I^0/\delta_I^c$  and  $\delta_{II}^0/\delta_{II}^c$  are assumed to be equal in the present study. For more information about the bilinear cohesive zone model, see Appendix B.

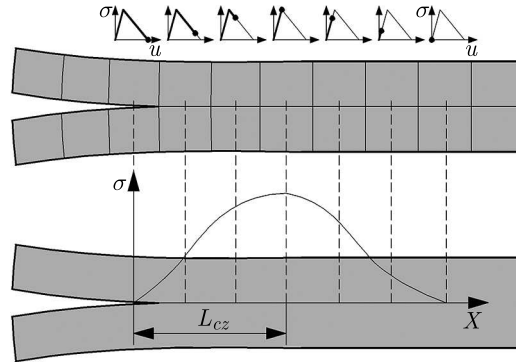


Fig. 4. Development of the fracture process zone

A model of the fracture process zone and its finite element implementation is shown in Fig. 4. The fracture process zone is a region ahead of the crack tip where the finite elements experience irreversible deformation. The numerical process zone length  $L_{cz}$  is calculated by adding the lengths of cohesive elements that are currently damaged  $L_{cz} = \sum l_i$ . In order to investigate the influence of cohesive strength on the load-deflection response and the process zone length of Norway spruce, parametric studies under mode I and mode II conditions have been conducted for experimentally established values of mode I and II fracture resistances  $G_{IR} = 0.286$  N/mm,  $G_{IIR} = 0.979$  N/mm (Phan *et al.*, 2016). It can be seen in Figs. 5a and 5b that as the cohesive strength increases, the peak load increases and the load-deflection response gets closer to the linear elastic solution obtained by using the simple beam theory. Details of the analytical solutions for the load-deflection response of the beam specimens can be found by Xie *et al.* (2016a). It should be noted that the analytical solutions are for the case of infinitely stiff interface with brittle failure ( $\delta_I^0$  and  $\delta_{II}^0 \rightarrow 0$ ,  $\sigma_I^0$  and  $\sigma_{II}^0 \rightarrow \infty$ ) and the observed deviation of

the initial stiffness from the linear elastic solution is typical for numerical simulations that use the bilinear cohesive zone model (e.g. Xie *et al.*, 2016b).

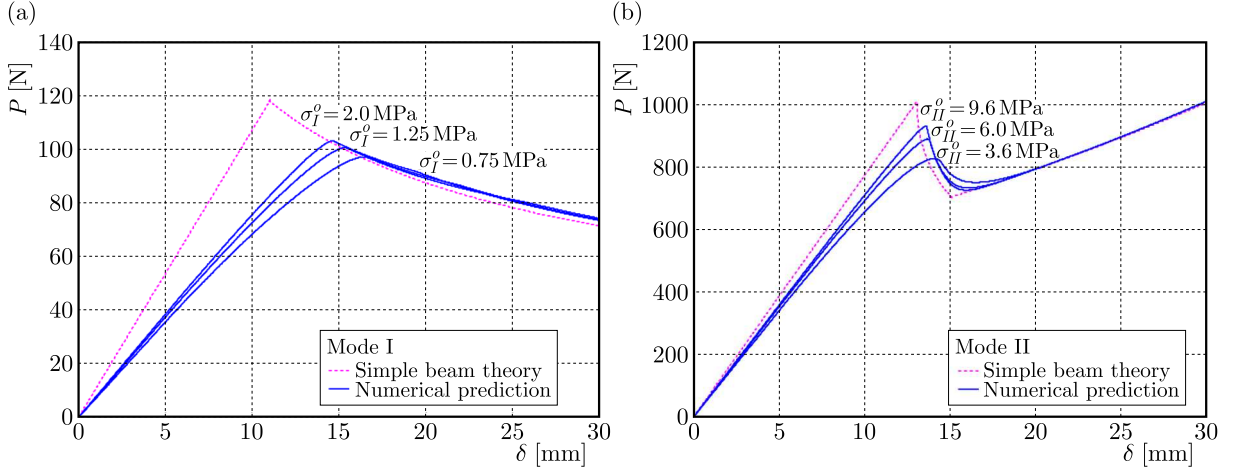


Fig. 5. Effect of cohesive strength on the load-displacement response for (a) mode I and (b) mode II loading

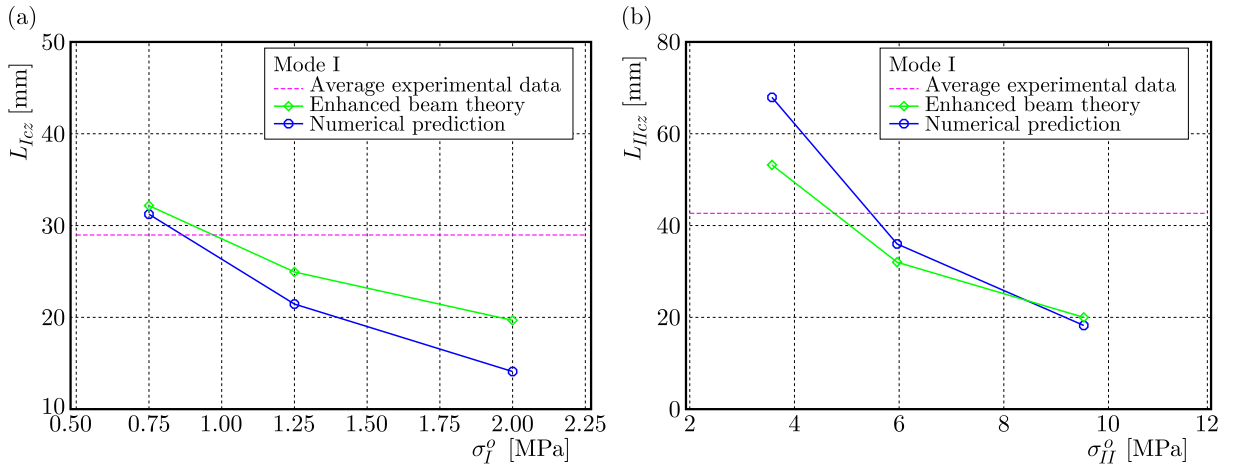


Fig. 6. Variation of the process zone length with cohesive strength for (a) mode I and (b) mode II loading (experimental data from Phan *et al.* (2016))

As shown in Figs. 6a and 6b, the process zone length, on the contrary, decreases with the increasing cohesive strength. This trend is found to agree with the analytical solution based on the enhanced beam theory (Xie *et al.*, 2016b)

$$L_{Icz} = \frac{1}{2} \sqrt[4]{\frac{E_{eff} G_{IR} h^3}{(\sigma_I^0)^2}} \quad L_{IIcz} = \frac{1}{2} \sqrt{\frac{E_{eff} G_{IR} h}{(\sigma_{II}^0)^2}} \quad (3.2)$$

where  $E_{eff} = E_L(1 - \nu_{LR}\nu_{RL})$  is found using the elastic constants (Table 1). Since the experimental load-deflection curves for Norway spruce are not available in Phan *et al.* (2018), the cohesive properties are calibrated in such a way that they satisfy equations

$$G_{IR} = \frac{1}{2} \sigma_I^0 \delta_I^c \quad G_{IIR} = \frac{1}{2} \sigma_{II}^0 \delta_{II}^c \quad (3.3)$$

and simultaneously the fracture process zone lengths predicted from the finite element models correspond closely to the reference values obtained from the experiments  $L_{Icz} = 29$  mm, and  $L_{IIcz} = 42.8$  mm (Phan *et al.*, 2016). Taking the above into account, the interface with

$\sigma_I^0 = 1.25$  MPa and  $\sigma_{II}^0 = 6$  MPa is chosen for the rest of the study. It is interesting to note that the adjusted value for the cohesive strength  $\sigma_I^0$  of Norway spruce is in good agreement with the literature data  $\sigma_I^0 = 1.66$  MPa (Dourado *et al.*, 2008) obtained for different specimen types. All cohesive properties used in the present study are summarized in Table 2.

**Table 2.** Cohesive properties of Norway spruce

$\sigma_I^0$ [MPa]	$\delta_I^0$ [mm]	$\delta_I^c$ [mm]	$\sigma_{II}^0$ [MPa]	$\delta_{II}^0$ [mm]	$\delta_{II}^c$ [mm]
1.25	0.04576	0.4576	6	0.03263	0.3263

Loads and deflections obtained from numerical simulations are processed with the compliance based beam method (CBBM) proposed by de Moura *et al.* (2010) to achieve mode I and II fracture resistances. CBBM is an example of the data reduction method which enables the determination of strain energy release rates on the assumptions of equivalent LEFM based on the theoretical specimen compliances

$$G_I = \frac{P_I^2}{2B} \frac{dC_I}{da} \quad G_{II} = \frac{P_{II}^2}{2B} \frac{dC_{II}}{da} \quad (3.4)$$

where  $P_I$ ,  $P_{II}$  are mode I and II components of the applied load,  $C_I$ ,  $C_{II}$  are mode I and II compliances,  $B$  is the specimen width. For more information about this method, see Appendix C.

#### 4. Results and discussion

In this Section, the theoretical and numerical predictions of the fracture resistance and the process zone length of Norway spruce under combined mode I and mode II loadings are compared with the experimental results reported by Phan *et al.* (2016). The key difference between experimental and numerical techniques for analyzing the crack growth resistance lies in the way of determining the crack length. In the experimental study performed by Phan *et al.* (2016), the crack length is calculated by setting the experimental specimen compliance to the relationship  $C(a) = \delta/P$  between the compliance and crack length obtained from a linear-elastic finite element analysis. In the present study, the crack length required by CBBM is estimated by setting the numerical specimen compliance to the compliance function  $C(a)$  derived from the beam theory (Appendix C).

Figures 7a and 7c show numerical predictions of the load-deflection and crack evolution curves by the cohesive zone model for different loading conditions. It is interesting to note that the crack starts to grow long before the peak load is reached. The observed pre-peak behavior is associated with the formation of the fracture process zone. The location of the transition point from stable to self-similar crack propagation on the crack evolution curve is found to appear just behind the peak load on the load-deflection curve. The critical loads are depicted by arrows in Figs. 7a-7c. It can be seen from these figures that the post-peak behavior under pure mode I loading differs from those under pure mode II and mixed-mode loading. In the case of pure mode I loading, the post-peak slope of both curves is almost constant, which is attributed to the self-similar crack growth regime. In the cases of pure mode II and mixed-mode loading, the post-peak slope of both curves changes because the specimens exhibit a load recovery when the crack approaches the central loading point,  $a = 325$  mm.

In the framework of equivalent LEFM, the crack stability is characterized by a resistance curve ( $R$ -curve) which indicates changes in the energy release rate as a function of crack length. Evolutions of the resistance to crack growth in Norway spruce obtained from CBBM for different loading conditions are shown in Figs. 8a-8c. They start from initial nonzero values of

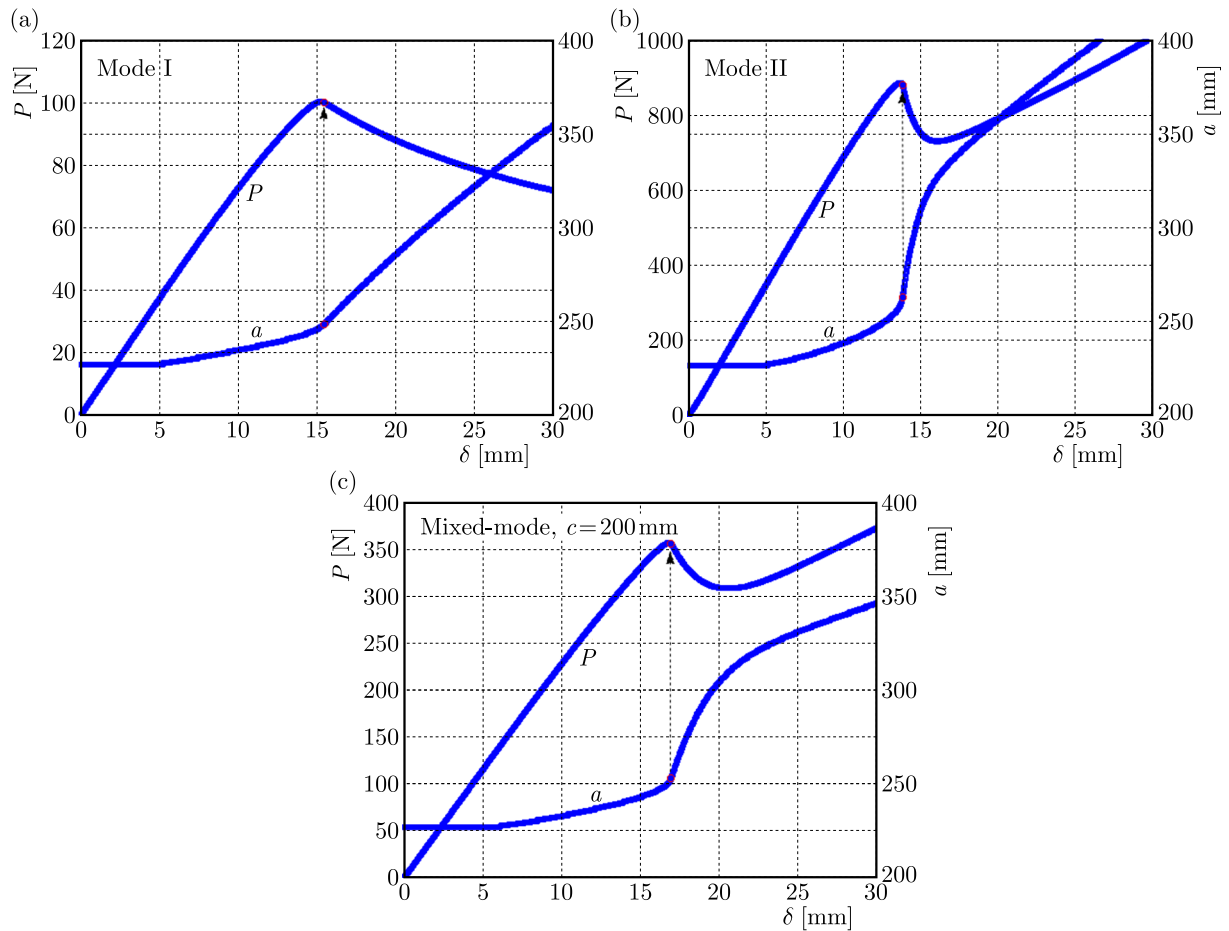


Fig. 7. The load-displacement and crack evolution curves from (a) DCB test, (b) ENF test and (c) MMB test

the energy release rate and consist of three distinct phases: the initial ascending phase followed by a plateau, and then another ascending phase. The numerical results are compared with the available experimental data (Phan *et al.*, 2016) to assess the performance of CBBM for the prediction of fracture resistance. Figure 9 compares the numerical predictions of  $R$ -curves obtained for the lever length  $c = 160$  mm using average material properties with the test data obtained from one specimen. It can be seen from this figure that CBBM fits the shape and magnitude of the experimental data reasonably well.

As discussed in the previous Section, fracture simulations using the cohesive zone model are capable of analyzing the development of the fracture process zone. The length of the process zone is calculated as the maximum distance between the centers of two cohesive elements located to the right of the current crack tip which have experienced damage. Numerical modeling of the process zone length in Norway spruce as a function of the crack length for different mixed-mode loading conditions is shown in Figs. 8a-8c. It can be seen that after the initial increase, the process zone length reaches for each loading case its maximum value and then remains constant over some increment of the crack length. The maximum value of the process zone length allows us to estimate the onset of self-similar crack propagation and, in this way, to clearly identify the point on the resistance curve where the fracture resistance is established. The fracture resistances are depicted by arrows in Figs. 8a-8c. The total fracture resistances  $G_R$  and the fully developed cohesive zone lengths  $L_{cz}$  calculated in this way for seven different mixed-mode ratios  $G_{II}/G$  are shown in Figs. 10 and 11, respectively.

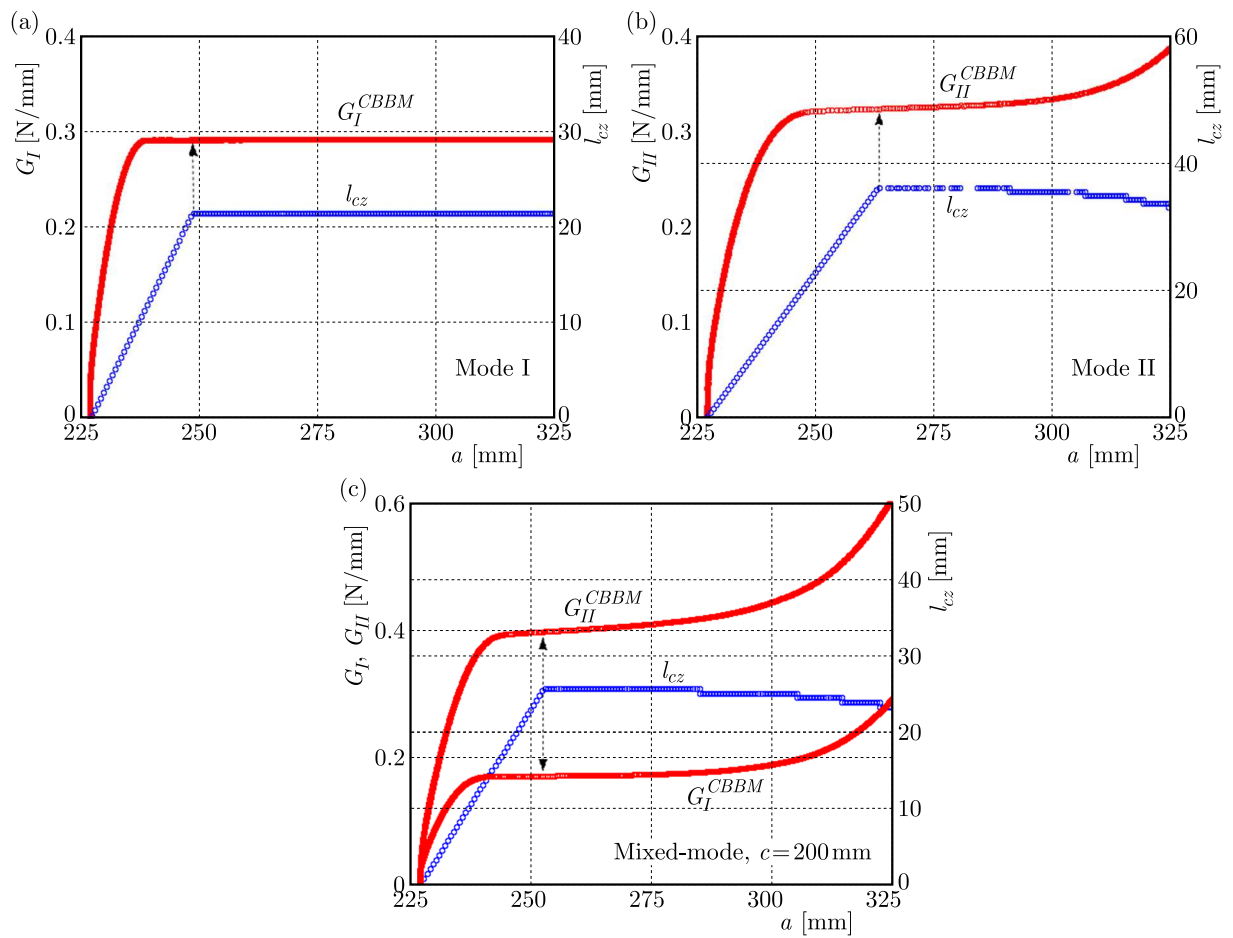


Fig. 8. The resistance curves and variations in the process zone length during crack propagation for (a) mode I, (b) mode II and (c) mixed-mode loading

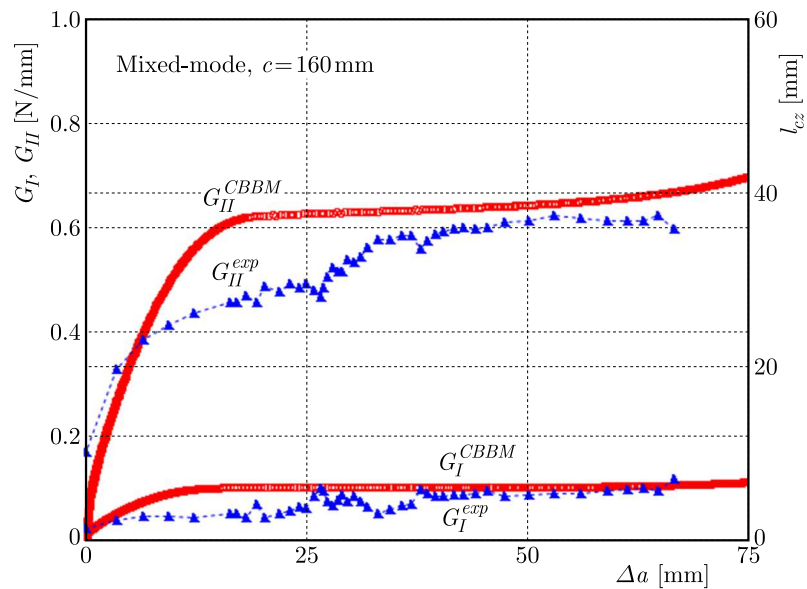


Fig. 9. Comparison between the predicted and measured resistance curves for  $c = 160$  mm (experimental data from Phan *et al.* (2016))

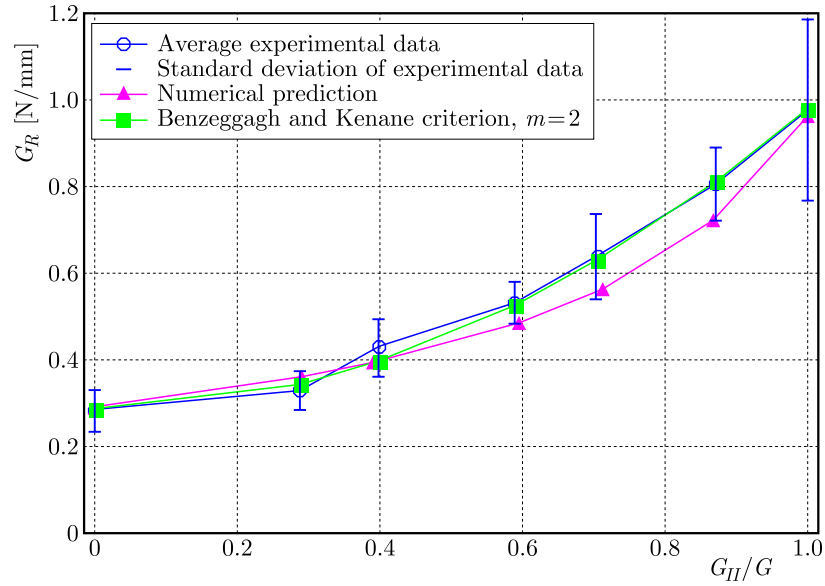


Fig. 10. Comparison between the predicted and measured fracture resistance of Norway spruce (experimental data from Phan *et al.* (2016))

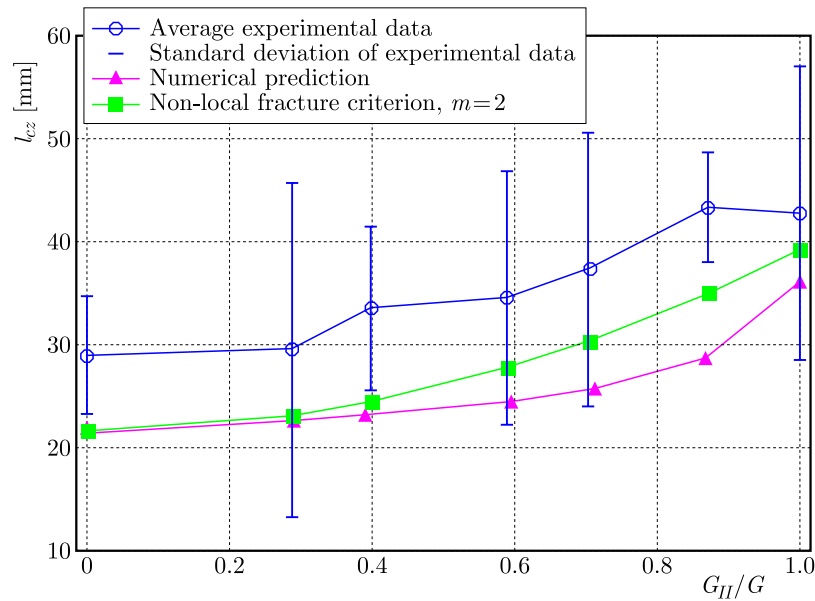


Fig. 11. Comparison between the predicted and measured process zone length of Norway spruce (experimental data from Phan *et al.* (2016))

Furthermore, Figs. 8a-8c show that it is only in the case of pure mode I loading that the specimen is capable of keeping the maximum value of the process zone length during the entire crack growth process. In the cases of pure mode II and mixed-mode loading, the process zone length beyond the maximum value decreases with the increasing crack length. This is because when the crack approaches the central loading point, the compressive stress zone at the center of the specimen disturbs the development of the fracture process zone. Thus, the development of the damage zone is influenced not only by the mixed-mode ratio but also by the specimen size. This finding sheds new light on the role of the scaling parameter  $n$  in the theoretical solution of the  $L_{cz}$  given by Eq. (2.10). It should be noted that there is a similarity between the theoretical and numerical solutions of the process zone length for pure mode I loading, namely that the

theoretical solution of the  $L_{Icz}$  is not influenced by the parameter  $n$ , whereas the numerical solution of  $L_{Icz}$  is free from the specimen size effect.

Figures 10 and 11 compare the theoretical and numerical predictions of the fracture resistance and critical process zone length of Norway spruce with the experimental data reported by Phan *et al.* (2016). The measured fracture resistance and critical process zone length of wood increase with an increase in the mixed-mode ratio. It can be seen from these figures that both the numerical prediction as well the analytical solution follow the trend of experimental points. In the case of the fracture resistance, the Benzeggagh and Kenane criterion with the parameter  $m$  taking the value of 2 is in a better agreement with the experimental data than the numerical prediction. In the case of the critical process zone length, the non-local fracture criterion with the parameter  $n$  taking the value of 3 provides a slightly better fit to the experimental data than the numerical prediction. The deviation of numerical predictions from experimental points is caused by the approximation of the true cohesive behavior of wood by the bilinear traction-separation law. The discrepancy between the theoretical predictions and experimental points is due to the fact that the fracture behavior is dependent not only on the specimen geometry and loading conditions but is also affected by the cohesion between the crack surfaces, which is not explicitly taken into account in the fracture criteria.

It should be noted that, similar to the parameter  $m$ , the parameter  $n$  is experimentally calibrated. Since the value of  $L_{Icz}$  is independent of  $n$ , only the value of  $L_{IIcz}$  is fitted in the calibration such that the shape of the theoretical curve describing the relationship between the process zone length and mixed-mode ratio matches the shape obtained experimentally. The value of mode II critical process zone length calculated for  $n = 3$  is  $L_{IIcz} = 39.2$  mm, whereas the same length obtained without scaling the compliance of the damage zone, for  $n = 1$ , has the value  $L_{IIcz} = 74.3$  mm, which is far from the measured value. This finding shows that the introduction of the parameter  $n$  into the non-local fracture model can be regarded as an advantage. The physical explanation of the parameter  $n$  is as follows. Since geometry of the body affects the development of the damage zone, it is reasonable to assume that the coalescence of microcracks in infinite bodies differs from that in slender bodies, such as beams. This means that the compliance of the damage zone depends on the specimen size and needs to be calibrated. Furthermore, it should be noted that a similar calibration procedure, as described above, is applied to the numerical model to estimate cohesive properties.

## 5. Conclusions

The applicability of non-local fracture theory to characterize fracture behavior of wood has been verified by comparing theoretical predictions with experimental data available in the literature and with numerical simulations accounting for cohesive properties of wood. The theoretical, numerical and experimental results presented in this paper have shown that not only the fracture resistance but also the process zone length depends nonlinearly on the mixed-mode ratio. The non-local fracture theory offers the ability to model the quasi-brittle fracture in wood without the need for using cohesive parameters which are difficult to estimate in practice. The concept of introduction of a scaling parameter into the non-local fracture theory has been proposed to take into account the specimen size effect on the development of the damage zone. The use of this scaling parameter has significantly improved the accuracy of the prediction of the critical process zone length. The ratio of the sliding and extensional compliance of the material within the damage zone has been defined as the ratio between the generalized elastic moduli, which has made it possible to achieve equivalence between the non-local and Benzeggagh and Kenane predictions of the fracture resistance. In this way, for the first time, the non-local theory has provided a physical explanation for the Benzeggagh and Kenane empirical criterion. The

comparison has shown that with much lower computational complexity, the proposed non-local model achieves a better efficiency than the numerical simulations.

#### Acknowledgement

The research described here was financially supported by the Ministry of Science and Higher Education of Poland under the grant No. WZ/WM-IIM/3/2020.

### Appendix A. Calculation of generalized elastic moduli

Following Sih *et al.* (1965), energy release rates can be related to stress intensity factors through generalized elastic moduli. Under plane strain conditions, the generalized elastic moduli  $E_I$  and  $E_{II}$  in the global coordinate system  $(x_1, x_2, x_3)$  aligned with the principal axes of orthotropy  $(L, T, R)$  are given by

$$E_I = \left[ \frac{S'_{11}S'_{22}}{2} \left( \sqrt{\frac{S'_{22}}{S'_{11}}} + \frac{2S'_{12} + S'_{66}}{2S'_{11}} \right) \right]^{-0.5} \quad E_{II} = \left[ \frac{(S'_{11})^2}{2} \left( \sqrt{\frac{S'_{22}}{S'_{11}}} + \frac{2S'_{12} + S'_{66}}{2S'_{11}} \right) \right]^{-0.5} \quad (\text{A.1})$$

where the constants  $S'_{11}$ ,  $S'_{12}$ ,  $S'_{22}$  and  $S'_{66}$  are related to components of the compliance matrix  $\{S_{ij}\}$  by

$$S'_{ij} = S_{ij} - \frac{S_{i3}S_{j3}}{S_{33}} \quad i, j = 1, 2, 6 \quad (\text{A.2})$$

where the compliance matrix  $\{S_{ij}\}$  relates the stress and strain components in the principal material directions according to generalized Hooke's law

$$\varepsilon_i = S_{ij}\sigma_j \quad i, j = 1, 2, \dots, 6 \quad (\text{A.3})$$

### Appendix B. Bilinear mixed-mode cohesive zone model

The behavior of the material in the cohesive zone is assumed to be linear-elastic up to the onset of damage, and after that, elastic damaging with linear softening is observed (Alfano and Crisfield, 2001; Camanho and Dávila, 2002). The constitutive relationships between stresses  $\sigma_i$  on the crack plane and the corresponding relative displacements  $\delta_i$  are as follows

$$\sigma_i = k_i(1 - d_i)\delta_i \quad i = I, II \quad (\text{B.1})$$

where  $k_i$  are the initial stiffness values and  $d_i$  are damage variables which satisfy the following conditions

$$d_i = \begin{cases} 0 & \text{when } \delta_i \leq \delta_i^0 \\ 1 & \text{when } \delta_i = \delta_i^c \end{cases} \quad (\text{B.2})$$

where  $\delta_i^0$ ,  $\delta_i^c$  are separations at the onset of damage and at the moment of fracture, respectively. When the material is under mixed-mode loading, the separation at damage onset is calculated based on the quadratic stress criterion

$$\left( \frac{\sigma_I}{\sigma_I^0} \right)^2 + \left( \frac{\sigma_{II}}{\sigma_{II}^0} \right)^2 = 1 \quad (\text{B.3})$$

where  $\sigma_I^0$  and  $\sigma_{II}^0$  are cohesive strengths. Using (B.3), the mixed-mode relative displacement corresponding to the onset of softening is given by

$$\delta_m^0 = \sqrt{(\delta_I^0)^2(\delta_{II}^0)^2 \frac{1 + \beta^2}{(\delta_{II}^0)^2 + \beta^2(\delta_I^0)^2}} \quad (\text{B.4})$$

where  $\beta = \delta_{II}/\delta_I$  is the mixed-mode ratio. The separation at fracture is calculated based on the linear energetic criterion

$$\frac{G_I}{G_I^c} + \frac{G_{II}}{G_{II}^c} = 1 \quad (\text{B.5})$$

where  $G_I^c$  and  $G_{II}^c$  are the critical strain energy release rates. Using (B.5), the mixed-mode relative displacement corresponding to total decohesion is given by

$$\delta_m^c = \frac{2(1 + \beta^2)}{\delta_m^0} \left( \frac{k_I}{G_I^c} + \frac{\beta^2 k_{II}}{G_{II}^c} \right)^{-1} \quad (\text{B.6})$$

### Appendix C. Equations of the compliance based beam method

In this paper, the strain energy release rates  $G_I$  and  $G_{II}$  are calculated using the Compliance Based Beam Method proposed by de Moura *et al.* (2010). Since the MMB test combines the DCB and ENF tests, equations for the strain energy release rate from these tests are used to calculate individual components of  $G$  for the MMB test. Mode I component is given by

$$G_I = \frac{6P_I^2}{B^2h} \left( \frac{2a_{eqI}^2}{E_{fI}h^2} + \frac{1}{5G_{LT}} \right) \quad (\text{C.1})$$

where  $a_{eqI}$  is the equivalent crack length in mode I estimated from the current specimen compliance

$$C_I = \frac{8a_{eqI}^2}{E_{fI}Bh^2} + \frac{12a_{eqI}}{5BhG_{LR}} \quad (\text{C.2})$$

and  $E_{fI}$  is the flexural modulus in mode I estimated from the initial specimen compliance  $C_{0I}$

$$E_{fI} = \frac{8(a_0 + \Delta)^3}{Bh^3} \left( C_{0I} - \frac{12(a_0 + \Delta)}{5BhG_{LT}} \right)^{-1} \quad (\text{C.3})$$

where  $a_0$  is the initial crack length,  $B$  and  $h$  are width and half-thickness of the specimen, respectively, constants  $\Delta$  and  $\Gamma$  are given by

$$\Delta = h \sqrt{\frac{E_{fI}}{11G_{LT}} \left[ 3 - 2 \left( \frac{\Gamma}{1 + \Gamma} \right)^2 \right]} \quad \Gamma = 1.18 \frac{\sqrt{E_{fI}E_T}}{G_{LT}} \quad (\text{C.4})$$

where  $E_L$ ,  $E_T$  and  $G_{LT}$  are the longitudinal, tangential and shear moduli, respectively. Mode II component is given by

$$G_{II} = \frac{(9P_{II}^2 a_{eqII}^2)}{16E_{fII}B^2h^3} \quad (\text{C.5})$$

where  $E_{fII}$  is the flexural modulus in mode II estimated from the initial specimen compliance  $C_{0II}$

$$E_{fII} = \frac{3a_0^3 + 2l^3}{8Bh^3} \left( C_{0II} - \frac{3l}{10G_{LT}Bh} \right)^{-1} \quad (\text{C.6})$$

and  $a_{eqII}$  is the equivalent crack length in mode II estimated from the current specimen compliance  $C_{II}$

$$a_{eqII} = \left[ \frac{C_{corrII}}{C_{0corrII}} a_0^3 + \frac{2}{3} \left( \frac{C_{corrII}}{C_{0corrII}} - 1 \right) l^3 \right]^{1/3} \quad (C.7)$$

where

$$C_{corrII} = C_{II} - \frac{3l}{10G_{LT}Bh} \quad C_{0corrII} = C_{0II} - \frac{3l}{10G_{LT}Bh} \quad (C.8)$$

The load  $P$  applied to the MMB test can be separated into mode I and mode II loading components as follows

$$P_I = \frac{3c-l}{4l} P \quad P_{II} = \frac{c+l}{l} P \quad (C.9)$$

where  $l$  is the half span length of the beam,  $c$  is the lever length.

## References

1. ALFANO G., CRISFIELD M.A., 2001, Finite element interface models for the delamination analysis of laminated composites: Mechanical and computational issues, *International Journal for Numerical Methods in Engineering*, **50**, 1701-1736
2. BARENBLATT G.I., 1962, The mathematical theory of equilibrium cracks in brittle fracture, *Advances in Applied Mechanics*, **7**, 55-129
3. BAZANT Z.P., KAZEMI M.T., 1990, Size effect in fracture of ceramics and its use to determine fracture energy and effective process zone length, *Journal of the American Ceramic Society*, **73**, 1841-1853
4. BENNATI S., FISICARO P., VALVO P.S., 2013a, An enhanced beam-theory model of the mixed-mode bending (MMB) test. Part I: Literature review and mechanical model, *Meccanica*, **48**, 443-462
5. BENNATI S., FISICARO P., VALVO P.S., 2013b, An enhanced beam-theory model of the mixed-mode bending (MMB) test. Part II: Applications and results, *Meccanica*, **48**, 465-484
6. BENZEGGAGH M.L., KENANE M., 1996, Measurement of mixed-mode delamination fracture toughness of unidirectional glass/epoxy composites with mixed-mode bending apparatus, *Composites Science and Technology*, **56**, 439-449
7. CAMANHO P.P., DÁVILA C.G., 2002, Mixed-mode decohesion finite elements for the simulation of delamination in composite materials, *Technical Report NASA/TM-2002-211737*, National Aeronautics and Space Administration, USA
8. DE MOURA M.F.S.F., OLIVEIRA J.M.Q., MORAIS J.J.L., XAVIER J., 2010, Mixed-mode I/II wood fracture characterization using the mixed-mode bending test, *Engineering Fracture Mechanics*, **77**, 144-152
9. DOURADO N., MOREL S., DE MOURA M.F.S.F., VALENTIN G., MORAIS J., 2008, Comparison of fracture properties of two wood species through cohesive crack simulations, *Composites Part A*, **39**, 415-427
10. DUGDALE D.S., 1960, Yielding of steel sheets containing slits, *Journal of the Mechanics and Physics of Solids*, **8**, 100-104
11. MOREL S., DOURADO N., VALENTIN G., 2005, Wood: a quasibrittle material.  $R$ -curve behavior and peak load evaluation, *International Journal of Fracture*, **131**, 385-400
12. MRÓZ Z., SEWERYN A., 1998, Non-local failure and damage evolution rule: Application to a dilatant crack model, *Journal of Physics IV*, **8**, 257-268

13. NOVOZHILOV V.V., 1969, On the necessary and sufficient criteria for brittle strength, *Prikladnaja Matematika i Mekhanika*, **33**, 212-222
14. OLIVEIRA J.M.Q., DE MOURA M.F.S.F., SILVA M.A.L., MORAIS J.J.L., 2007, Numerical analysis of the MMB test for mixed-mode I/II wood fracture, *Composites Science and Technology*, **67**, 1764-1771
15. PEDERSEN M.U., CLORIUS C.O., DAMKILDE L., HOFFMEYER P., 2003, A simple size effect model for tension perpendicular to the grain, *Wood Science and Technology*, **37**, 125-140
16. PHAN N.A., MOREL S., CHAPLAIN M., 2016, Mixed-mode fracture in a quasi-brittle material: R-curve and fracture criterion: Application to wood, *Engineering Fracture Mechanics*, **156**, 96-113
17. REEDER J.R., CREWS J.H., 1990, Mixed-mode bending method for delamination testing, *AIAA Journal*, **28**, 1270-1276
18. ROMANOWICZ M., 2019, A non-local stress fracture criterion accounting for the anisotropy of the fracture toughness, *Engineering Fracture Mechanics*, **214**, 544-557
19. SEWERYN A., MRÓZ Z., 1998, On the criterion of damage evolution for variable multiaxial stress states, *International Journal of Solids and Structures*, **35**, 1589-1616
20. SIH G.C., PARIS P.C., IRWIN G.R., 1965, On cracks in rectilinearly anisotropic bodies, *International Journal of Fracture Mechanics*, **1**, 189-203
21. WANG Y., WILLIAMS J.G., 1992, Corrections for mode II fracture toughness specimens of composites materials, *Composites Science and Technology*, **43**, 251-256
22. WILLIAMS J.G., 1989, End corrections for orthotropic DCB specimens, *Composites Science and Technology*, **35**, 367-376
23. XIE D., BIGGERS S.B., 2006, Progressive crack growth analysis using interface element based on the virtual crack closure technique, *Finite Elements in Analysis and Design*, **42**, 977-984
24. XIE J., WAAS A.M., RASSAIAN M., 2016a, Closed-form solutions for cohesive zone modeling of delamination toughness tests, *International Journal of Solids and Structures*, **88-89**, 379-400
25. XIE J., WAAS A.M., RASSAIAN M., 2016b, Estimating the process zone length of fracture tests used in characterizing composites, *International Journal of Solids and Structures*, **100-101**, 111-126

*Manuscript received October 30, 2022; accepted for print November 29, 2022*